

https://doi.org/10.1070/QEL17021

Modelling an electro-optical modulator based on a vertical p–n junction in a silicon-on-insulator structure

A.V. Tsarev, R.M. Taziev

Abstract. **We report the results of numerical simulation of a Mach–Zehnder electro-optical modulator using beam splitters based on multimode interference in a silicon-on-insulator structure. The control is provided due to the depletion effect in the vertical p–n junction, which can be fabricated using the self-alignment technology. An optimal modulator design is proposed, which impedance is matched with an external 50-Ω load, for which, with a reverse bias of –5 V and an active length of 1.7 mm, the optical frequency bandwidth of ~ 50 GHz can be achieved. A special doping profile of the p–n junction of the modulator is presented, which provides an optical frequency bandwidth of 30 GHz with a reverse bias of –3 V and a modulator length of 2.5 mm. Such modulators can be used in integrated optics, optical communications and radio photonics devices.**

Keywords: *electro-optical modulator, silicon-on-insulator, p–n junction, numerical simulation, integrated optics, radio photonics.*

1. Introduction

Integrated optics and nanophotonics technologies belong to critical technologies without which the development of the information society is impossible. With their help, significant progress was achieved in technical parameters (efficiency, miniaturisation, operating speed, etc.) of optoelectronic elements and systems for optical communication, radio photonics and data processing and transmission systems. Microwave electro-optical (EO) modulators underlie many elements of radio photonics. The modulator operation is based on the matched coupling of microwave and optical waves in an electrode structure and optical waveguide in the optoelectronic device, in which the amplitude or phase of an optical wave changes under the influence of applied microwave electric voltage.

Historically, the most common EO modulators are based on lithium niobate [1–3]. They allow operating at frequencies up to 40 GHz. The technology of their manufacturing is well established – they are reliable and heat-resistant; however, they have large length and suffer from a significant limitation on the operating frequency of microwave modulation.

A.V. Tsarev Rzhanov Institute of Semiconductor Physics, Siberian Branch, Russian Academy of Sciences, prosp. Akad. Lavrent'eva 13, 630090 Novosibirsk, Russia; Novosibirsk State University, ul. Pirogova 2, 630090 Novosibirsk, Russia; e-mail: tsarev@isp.nsc.ru;
R.M. Taziev Rzhanov Institute of Semiconductor Physics, Siberian Branch, Russian Academy of Sciences, prosp. Akad. Lavrent'eva 13, 630090 Novosibirsk, Russia; e-mail: taziev@isp.nsc.ru

Received 22 March 2019; revision received 24 April 2019
Kvantovaya Elektronika **49** (11) 1036–1044 (2019)
Translated by V.L. Derbov

To achieve a modulator frequency band of the order of 100 GHz, modern electro-optical polymers with a high electro-optical coefficient (exceeding 100 pm V^{-1}) can be used [4]. The best values of the control voltage and the achieved frequency band were implemented in hybrid silicon modulators operating in the travelling-wave regime using silicon slot waveguides and/or photonic crystals filled with an electro-optical polymer [5, 6]. The disadvantage of such modulators is the necessity to work with a low level of optical power of the transmitted signal (due to the high energy density in the slot waveguide), which is critical for radio photonics devices.

An alternative solution is to use all-polymer electro-optical modulators based on ridge waveguides [7–13], which have a large cross section of the optical mode and, therefore, can operate at optical power two orders of magnitude larger [11] than that of silicon slot waveguides. Unfortunately, due to the lower control efficiency, these modulators also have a relatively large length (several centimetres), which leads to significant values (several volts) of the control voltage due to losses of the microwave wave and the velocity mismatch between the optical and microwave waves in the structure of the modulator operating in the travelling-wave regime. Based on numerical experiments, we showed [14] that by using MgO dielectric strips having a high dielectric constant, it is possible to reduce significantly (up to 2.8 times) the half-wave control voltage, when operating in the frequency band of ~100 GHz. Unfortunately, the technology of MgO film production is optimised for ultrathin (1–100 nm) layers, and the fabrication of films of required thickness (several microns) is a challenging technological problem that impedes the practical realisation of the advantages of this concept of electro-optical modulators.

Modulators based on the quantum-confined Stark effect in layered structures with multiple quantum wells [15–17] grown using layer-by-layer epitaxy on indium phosphide (InP) substrates are very promising. They are implemented in very compact optical elements and, in addition, they can be grown in a monolithic structure together with sources or receivers of optical radiation. The main disadvantage of such modulators is the high cost of their manufacture.

A good alternative platform for producing microwave modulators is silicon photonics, which in the last decade has become one of the most popular technologies for the development and manufacture of photonic elements and devices [18–33]. Its undoubted advantage is high compatibility with the CMOS technology of micro- and nanoelectronics, as well as the practical possibility of implementing most of the basic components of monolithic integrated-optical circuits on a single technological platform. Currently, intensive develop-

ment of a laser radiation source and an electro-optical modulator in silicon-based integrated design is underway, but we do not consider this problem here.

2. Statement of the problem

Analysis of modern scientific literature shows that the vast majority of silicon electro-optical modulators are manufactured based on silicon-on-insulator (SOI) structures in which the optical waveguide is located on a thick (~2 μm) buried oxide layer [18–25]. Such a layer provides optical isolation from a silicon substrate on which a microwave modulator is formed, which is an independent optical element or part of a more complex optical integrated circuit.

The technology for the development of silicon electro-optical modulators has come a long way from low frequency cells operating on injection of charge carriers to microwave cells that can operate at frequencies up to 40 GHz and are an order of magnitude smaller than similar modulators based on lithium niobate. The operating speed of such elements is provided by the operation of the p–n junction in the depletion regime, as well as by the application of a travelling-wave modulator circuit.

The electro-optical control of the semiconductor modulator is implemented by changing the concentration of free carriers [26] in the region of the p–n junction of the waveguide, where the optical wave propagates. In this case, the complex propagation constant of the optical mode changes, which leads to the dependence of the amplitude and phase of the optical wave on the control voltage. For the operation of the modulator, as a rule, phase modulation of the wave is used. To convert phase modulation to amplitude one, structures like a ring resonator or modulators based on a Mach–Zehnder interferometer are usually exploited. The former possess small size, but require precise control of the radiation wavelength at which the modulator operates. The latter are large (up to several millimetres), but are able to work in a wide range of wavelengths and are less sensitive to temperature changes. To reduce the control voltage by a factor of two, a push–pull modulator is used, in which the microwave modulates in antiphase the waves in two arms of the Mach–Zehnder interferometer.

Typically, silicon modulators are based on a horizontal p–n junction [24], whose characteristics are very sensitive to the accuracy of its positioning across the waveguide ridge, which has a small characteristic size (0.5–0.6 μm). Recently, a modulator design has been proposed based on a vertical p–n junction [27–32], manufactured using the self-alignment process [30]. The achievable operating frequency band of modulators with vertical p–n junctions is significantly inferior to that of modulators with horizontal p–n junctions [33]. Nevertheless, if we solve the problem of increasing the operating frequency band of modulators with a vertical p–n junction, their higher efficiency [33] and more reproducible manufacturing technology will make the efforts to develop modulators at vertical p–n junctions justified from the point of view of their practical use.

In this work, we performed a numerical analysis and optimised the parameters of electro-optical microwave modulators based on the SOI vertical p–n junction. This allowed determination of the structural parameters of the modulator, providing both a small value of the control voltage and a wide band of operating frequencies, comparable with the bands of the best modulators with horizontal p–n junctions. To reduce the control voltage and match the modulator impedance with a 50-Ω load, an original donor doping profile of the semiconductor is proposed, in which the waveguide ridge has a low concentration of free charge carriers (electrons), and the region adjacent to the ridge has a high concentration of charge carriers. Numerical modelling was performed using the specialised commercial software package RSoft [34] with the MultiPhysics Carrier Utility for calculating the perturbation of the refractive index in a semiconductor structure when it is modulated by an external electric field. To model the microwave properties of the active part of the modulator, where light is modulated by microwave radiation, specialised software packages can be used, for example, CST Microwave Studio [35] or ANSYS HFSS [36]. In this work, we used the microwave package ANSYS HFSS.

3. Optical properties of the Mach–Zehnder interferometer

The classical scheme of the Mach–Zehnder interferometer was chosen as the modulator optical scheme. Such a scheme

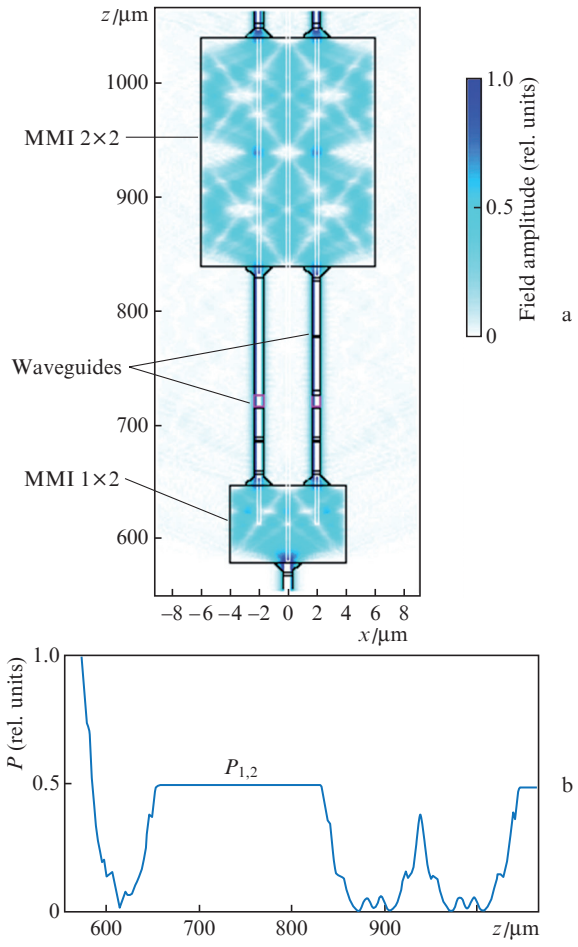

Figure 1. (a) Optical scheme of the Mach–Zehnder interferometer using MMI elements 1 × 2 and 2 × 2, as well as the transverse distribution of the field amplitude of the optical wave as it propagates and (b) power change relative to the input signal level for the fundamental mode as it propagates through the structure for the left (P_1) and right (P_2) arms of the Mach–Zehnder interferometer (coincident for a zero phase shift of the waves in the arms of the interferometer). The calculation was carried out using the three-dimensional beam propagation method (3D BPM).

converts a controlled variation of phase of an optical wave propagating through the p–n junction region into the amplitude modulation at the output of the interferometer. The Mach–Zehnder interferometer itself uses multimode interference (MMI) beam splitters, namely, a 1×2 MMI beam splitter at the input of the device, and a 2×2 MMI beam splitter at the output (Fig. 1). A distinctive property of this optical scheme is that the interferometer is at the operating point (equal amplitudes of the left and right channels) when the phase difference between the optical waves in different arms at the output of the interferometer is zero. In addition, this scheme is characterised by low insertion loss, high resistance to manufacturing errors and broad band of operating wavelengths (Fig. 2). All numerical analysis was performed for a single-mode optical ridge waveguide in a silicon-on-insulator structure with a ridge having the width and height of 600 and 200 nm, respectively, located on a planar base 200 nm thick, separated from the silicon substrate by an oxide buffer layer 2 μm thick.

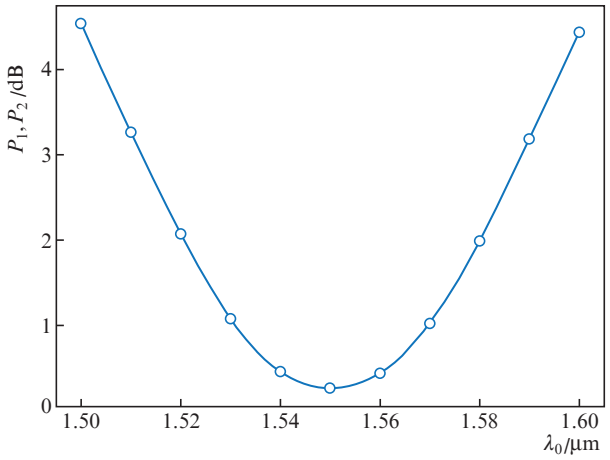

Figure 2. Spectral dependence of the optical power P_1 and P_2 at the output of the Mach–Zehnder interferometer (see Fig. 1). 3D BPM calculation.

It is known that silicon has high nonlinearity, which can lead to spurious effects even at a moderate power of transmitted radiation [37]. To reduce it, we selected a structure with a larger cross section than usual. In addition, a planar base 200 nm thick is optimal for the manufacture of grating coupling elements, and the fundamental mode of this ridge waveguide with negligible losses can be transformed using an inverted wedge into a wide beam distributed in a planar base [38], for subsequent input into a single-mode optical fibre using diffraction gratings.

The efficiency of electro-optical control using the p–n junction with reverse bias is known to decrease with increasing size of the waveguide, because the relative variable part of the depletion region decreases. However, the present paper shows that the waveguide structure with parameters chosen by us has very good characteristics for fabricating promising types of silicon-based electro-optical modulators.

4. Optical properties of a vertical p–n junction

A schematic of the structure of the vertical p–n junction of the modulator is shown in Fig. 3. The manufacturing technol-

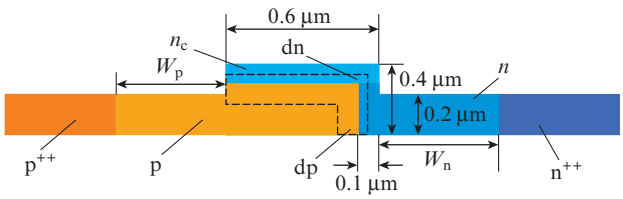

Figure 3. Cross section of doping regions of an electro-optical modulator based on a vertical p–n junction.

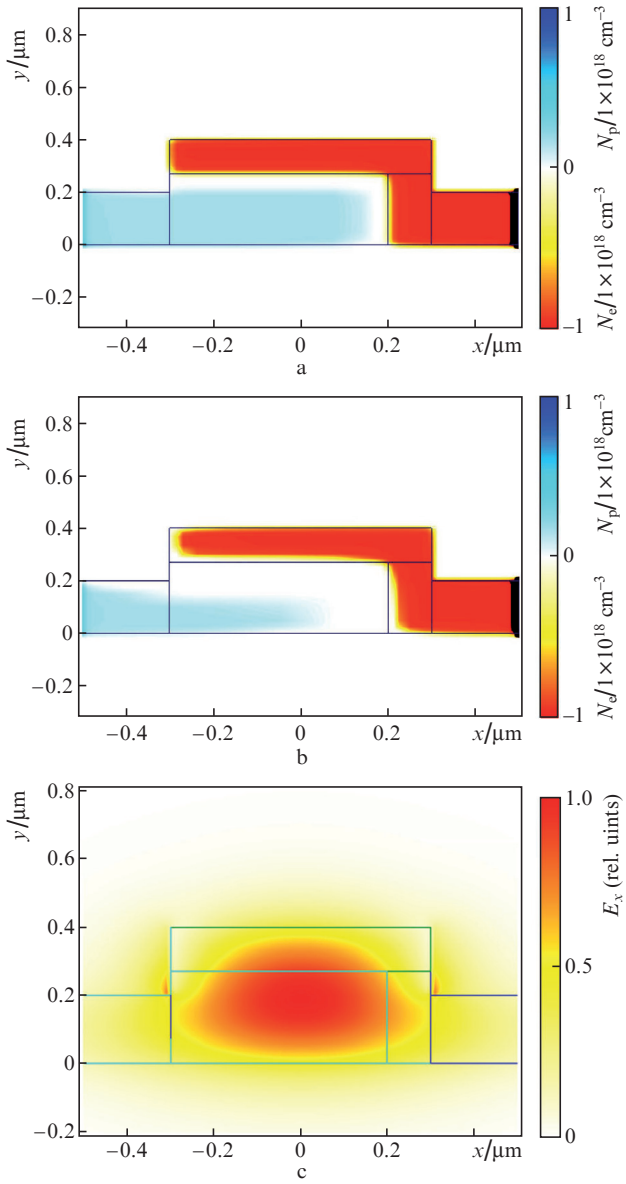

Figure 4. (Colour online) Distributions of concentrations of free charge carriers for (a) zero bias voltage and (b) bias voltage of –5 V for holes (N_p) and electrons (N_e), as well as (c) the transverse distribution of the fundamental mode field of a ridge waveguide for zero bias voltage at $N_A = 3 \times 10^{17}$ cm^{-3}, $N_D = 14 \times 10^{17}$ cm^{-3}. 3D BPM calculation.

ogy of such structures is described in Refs [30–32]. In this case, it is a ridge waveguide on a p-type substrate in which additional regions of p^{++} and n^{++} types are formed. We are interested in the optical properties of these structures, which depend on the concentration of donor and acceptor impuri-

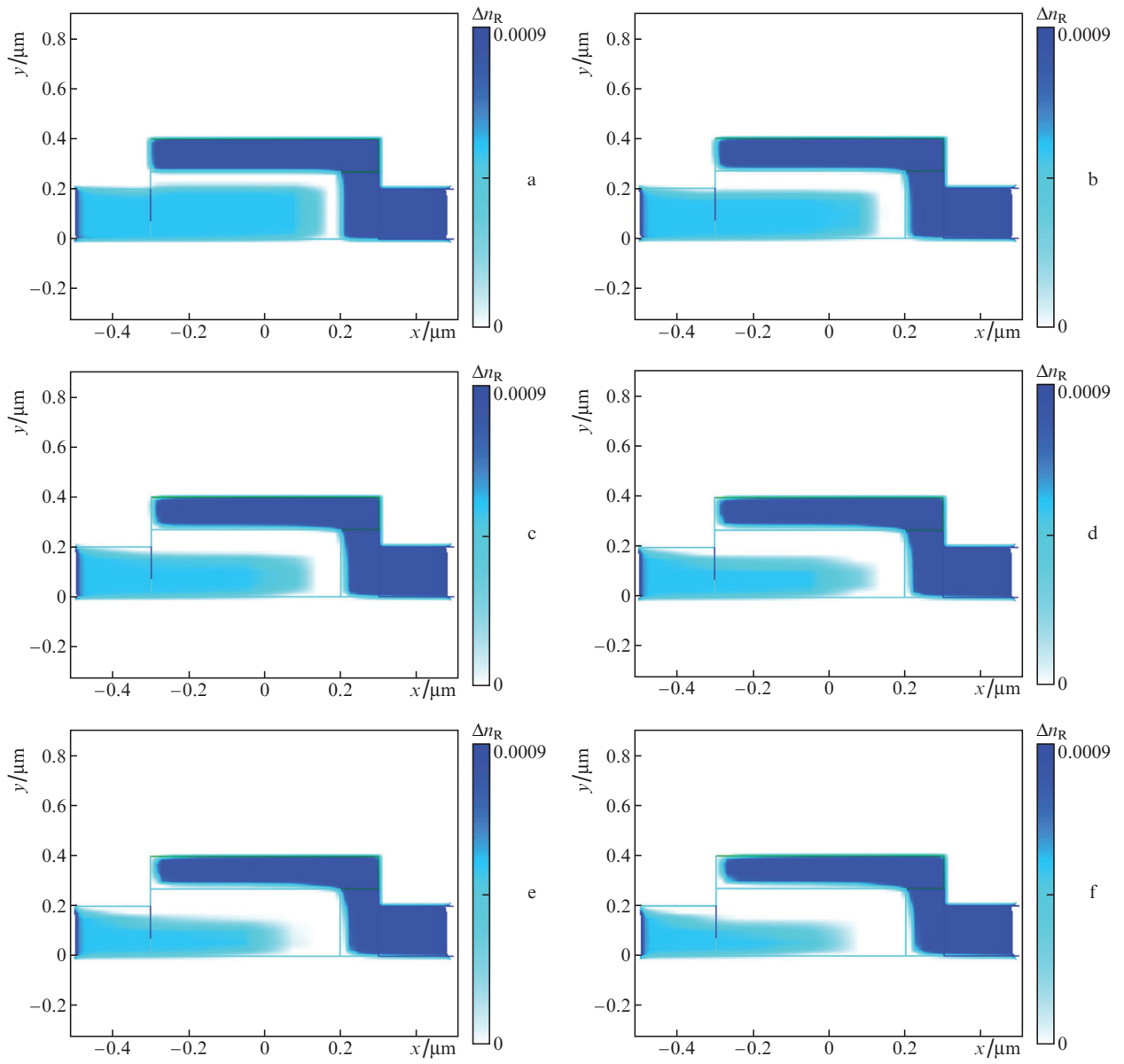

Figure 5. (Colour online) Transverse distribution of the perturbation of the real part of the refractive index for reverse bias voltages V = (a) 0, (b) 1, (c) 2, (d) 3, (e) 4 and (f) 5 V; $N_A = 3 \times 10^{17}$ cm^{-3}, $N_D = 14 \times 10^{17}$ cm^{-3}. Calculation using the optical package from RSoft.

ties, geometric parameters and physical properties of the SOI structure.

In the calculation process, the electric potential distribution is first found taking into account the doping level of all layers, and then the changes in the real and imaginary parts of the refractive index, which depend on the concentration of free charge carriers, are calculated. Then we analyse the propagation of the optical waves and microwaves through the waveguide structure, whose properties are controlled by an external electric field.

Calculations performed using the RSoft package show that the optical properties of these structures can be efficiently controlled by an external electric field, which causes significant changes in the real and imaginary parts of the refractive index for the mode propagating through the waveguide. The physical reason for these changes is that with a variation in the control voltage, the size of the depletion regions (denoted in Fig. 3 by dn and dp for electrons and holes, respectively), which are responsible for the change in the refractive index associated with the concentration of free carriers, changes significantly [26]. In particular, Fig. 4 shows the transverse distributions of the concentrations of free charge carriers (holes and electrons) for two different values of the control voltage. For the optimal modulator design, the maximum values of the fundamental mode field of the optical waveguide (Fig. 4c) coincide with the region of the maximum change in the concentration of free carriers (Fig. 4a, Fig. 4b) and, therefore, with the region of the maximum change in the refractive index (Fig. 5). All this provides high efficiency of electro-optical control of the phase of the optical wave in a silicon optical waveguide.

Our task is to find such parameters of the structure shown in Fig. 3, which provide a significant change in the phase of the optical wave during its propagation in the waveguide with a relatively small attenuation of the optical wave and microwave in order to obtain a wide microwave modulation band.

The attenuation of a microwave depends quadratically on the frequency and electric capacitance of the p–n junction, which, in turn, depends both on the doping level and on the electric potential of the reverse bias at the p–n junction. Besides that, the attenuation of the optical wave depends on the geometry of the cross section of the optical waveguide. As shown by numerical studies conducted in many laboratories, the doping parameters that are optimal to achieve the minimum attenuation and maximum phase change of the optical wave are not optimal for the parameters of the microwave. Hence, the problem is multi-parameter and does not have a unique solution, because the optimisation of parameters affects the properties of optical and microwave radiation in the opposite way. The only way to overcome this contradiction is to find suboptimal ('compromise') doping parameters to reduce the attenuation of the optical wave and microwave that can be used to solve a specific practical problem.

It is known [32] that from the point of view of controlling the phase of the optical wave, holes are preferable to electrons, because they cause smaller attenuation of the optical wave [26]. Therefore, holes in silicon electro-optical modulators usually occupy a large part of the structure in the localisation region of the waveguide optical mode. In addition, to control the size of the depletion region better, the electron concentration should be greater than that of the holes. Both these factors were taken into account in our calculations, in which we changed the doping level of acceptors N_p (to control the concentration of free holes) and donors, N_n (to control the concentration of free electrons). In the numerical analysis, we used a uniform distribution of the doping profile over the thickness of the p–n junction structure, typical of the self-alignment technological procedure [30]. The latter consists in first doping with acceptors to form a planar base with hole conductivity and producing an additional thin n-type top layer (with a concentration of free carriers n_c). Then a mask is formed, through which the waveguide ridge is formed by etching, and then through the same mask by donor ion implantation (at an angle to the surface) a hole-enriched layer (with a concentration of free carriers n) is formed to the right of the ridge in the planar base (see Fig. 3). Heavily doped regions of p^{++} and n^{++} types and control electrodes are formed during subsequent technological operations.

We are interested in suboptimal concentrations of donors and acceptors in the p–n junction region. Heavily doped p^{++} and n^{++} regions are far from the localisation region of the fundamental waveguide mode and weakly affect the efficiency of electro-optical interaction. They are necessary for forming electrical contacts and their properties are insignificant when solving the problem of optimising the electrophysical parameters of the modulator.

To describe the optical properties of the modulator, two main parameters were used as critical ones: first, the characteristic length $L_{\pi/2}$ of the phase-shifting element of the modulator and, second, the corresponding attenuation $L_{loss\,\pi/2}$ of the optical wave, necessary to shift its phase by $\pi/2$, which corresponds to the complete switching of the push-pull modulator signal at a given voltage V between the domains n^{++} and p^{++}. It is known that the characteristic of this type of the electro-optical modulator is nonlinear (Fig. 6); therefore, the optimisation of the parameters of the electro-optical modulator should be carried out taking into account its geometry, estimated operating voltage, and also the required operating frequency band. Our calculations were performed for the modulator structure corresponding to that shown in Fig. 3.

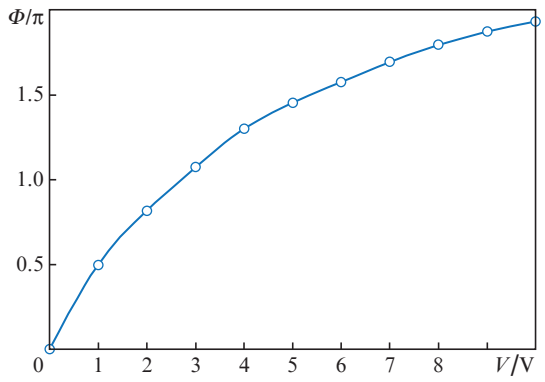

Figure 6. Phase incursion Φ in the arm of a Mach–Zehnder interferometer 5 mm long as a function of reverse bias voltage V applied to the n^{++} region of the electro-optical modulator based on the vertical p–n junction with uniform doping. The electric potential in the p^{++} region is zero, $N_A = 3 \times 10^{17}$ cm^{-3}, $N_D = 14 \times 10^{17}$ cm^{-3}. Calculation using the optical package from RSoft.

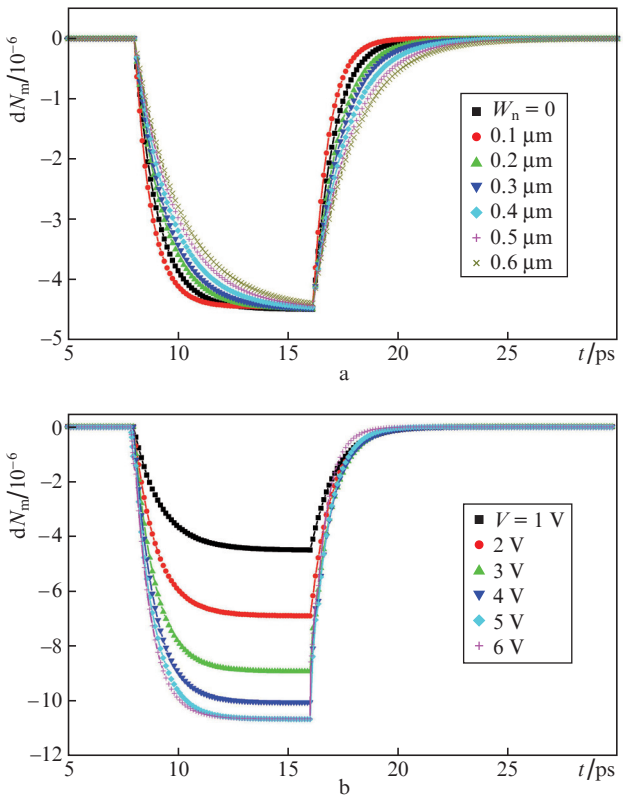

Figure 7. (Colour online) Time dependences of the effective refractive index dN_m for the fundamental mode when a short voltage pulse with an amplitude of 0.5 V is applied for (a) different sizes of the doping region beyond the ridge boundaries ($W_n = W_p$) and (b) different values of the reverse bias voltage V at $W_n = W_p = 0.2$ μm; $N_A = 3 \times 10^{17}$ cm^{-3}, $N_D = 14 \times 10^{17}$ cm^{-3}. Calculation using the optical package from RSoft.

Note that the modulator operation is considerably influenced by the size of the regions doped with holes and electrons (W_p and W_n regions), adjacent to the waveguide ridge (Fig. 3) and separating it from the heavily doped p^{++} and n^{++} regions, where the control electrodes will be located. In particular, the parameters W_p, W_n, p, n and n_c significantly affect the frequency characteristics of the modulator. For illustra-

tion, Fig. 7 shows the calculated time dependences of the effective refractive index for the fundamental mode under the influence of a short voltage pulse with an amplitude of 0.5 V. For example, it can be seen that the response time of the vertical p–n junction decreases to 1 ps, when W_n decreases from 0.6 to 0.2 μm. A further decrease in W_n and W_p is impractical due to a significant increase in optical losses as the heavily doped p^{++} and n^{++} regions approach the localisation region of the fundamental waveguide mode (see Fig. 5). Therefore, in what follows, we used the value $W_n = W_p = 0.2$ μm, which provides a sufficiently fast response of the p–n junction to a change in the electric field over the entire range of the bias voltages applied to the junction (Fig. 7b). In turn, this leads to a wide operating band of the p–n junction, calculated with a small change in the signal amplitude. Note that the frequency dependence of the change in the refractive index of the p–n junction is described with good accuracy by a combination of the Gaussian function and the exponential function:

$$M_{pn}(F) = y_0 + A_1\exp(-(F/t_1)^2) + A_2\exp(-F/t_2), \quad (1)$$

where F is the frequency in gigahertz.

The fitting parameters found from the dependences shown in Fig. 8 are given in Table 1. They also allow finding the maximum width of the optical operating frequency band [39] of the p–n junction ΔF_{pn}, determined from the relation $M_{pn}(\Delta F_{pn}) = 0.5$.

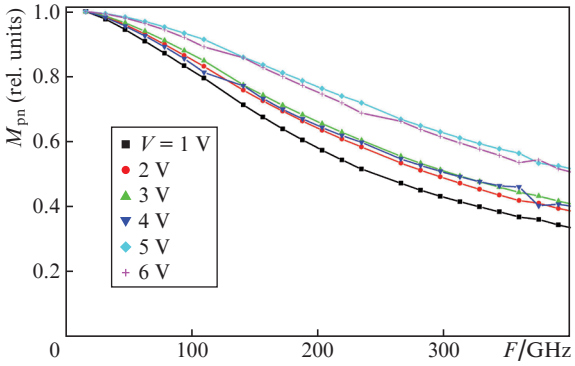

Figure 8. Relative change in the refractive index of the p–n junction for the fundamental mode vs. the frequency of the weak modulating signal applied to the electrode structure of the p–n junction operating in the depletion regime; $N_A = 3\times10^{17}$ cm^{-3}, $N_D = 14\times10^{17}$ cm^{-3}. Calculation using the optical package from RSoft.

Table 1. Parameters for approximating the frequency response of a vertical p–n junction.

Parameters	V/V						
	1	2	3	4	5	6	7
y_0	0.053	0.058	0.0655	0.0722	0.0883	0.101	0.108
A_1	0.374	0.342	0.3127	0.3611	0.2201	0.312	0.362
t_1/GHz	196.0	222.6	229.6	233.1	301.2	294.2	257.4
A_2	0.584	0.614	0.6431	0.5623	0.7341	0.607	0.557
t_2/GHz	524.1	581.3	576.9	652.7	639.6	726.6	725.2
ΔF_{pn}/GHz	243	285.3	303.5	297.1	420.4	400	358.3

We calculated the main parameters of the electro-optical modulator [characteristic length $L_{\pi/2}$ and optical losses $L_{loss\,\pi/2}$ (Fig. 9)], at which a phase shift of π/2 is achieved in the course of propagation of an optical wave through a ridge waveguide with a p–n junction. They are determined by calculating the real and imaginary parts of the effective refractive index for the fundamental mode and substantially depend on the concentration of dopants and, especially, on the bias voltage.

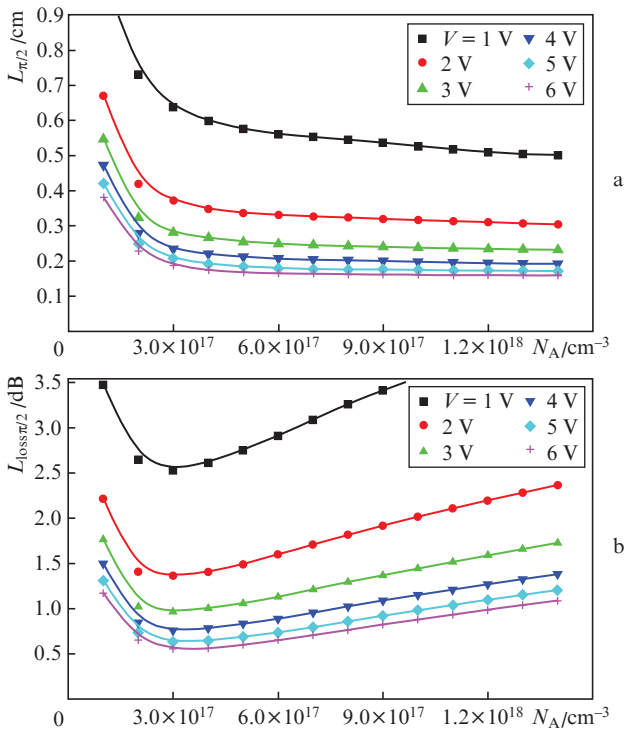

Figure 9. Dependence of (a) length and (b) optical losses providing a phase shift of π/2 on the concentration of acceptors for various values of reverse bias voltage at the p–n junction operating in the depletion regime; $N_A = 3\times10^{17}$ cm^{-3}, $N_D = 14\times10^{17}$ cm^{-3}. Calculation using the optical package from RSoft.

As already noted above, based only on optical calculations (see Figs 8 and 9) we cannot draw a conclusion about the optimal design parameters of a microwave-range EO modulator, because in this case a decisive role is played by its microwave properties, mainly the attenuation and propagation velocity of the microwave. In particular, the results presented in Fig. 9 show that it is desirable to use a donor concentration of $N_D = 3\times10^{17}$ cm^{-3}, because in this case, a minimum of optical losses is observed and a moderate control efficiency of the optical wave phase is achieved. However, a joint consideration of all factors (taking the microwave properties of the structure into account) showed that the suboptimal parameters for the broadband EO modulator are the concentrations of acceptors, $N_A = 3\times10^{17}$ cm^{-3}, and donors, $N_D = 14\times10^{17}$ cm^{-3}. Such a concentration of donors is due to the need to reduce the ohmic resistance of the n-type region adjacent to the p–n junction, without which it is impossible to provide a sufficiently wide microwave modulation band.

5. Microwave properties of the vertical p–n junction

To model the microwave properties of the active part of the modulator, where the microwave modulates the light wave, a

specialised software package for microwave simulations was used [36]. The widths of the modulator electrodes were varied to achieve the impedance of the coplanar line close to 50 Ω at the operating voltage, as well as to reduce losses during the propagation of the microwave. The distance between the centres of two optical waveguides on a silicon substrate was chosen to be 8 μm, which corresponds to the parameters of the optical scheme of the Mach–Zehnder interferometer (see Fig. 1).

As follows from the results of the study of silicon modulators described in the literature, the impedance of the coplanar line of the modulator is usually 25–35 Ω. Therefore, it is necessary to control the two arms of the silicon modulator in such a way that the current would flow in them in series. Such a series connection of the p–n junctions of the modulator essentially simplifies the task of obtaining a 50-Ω impedance of the coplanar microwave line. In this case, the phase-shifting elements operate in the push–pull regime, in which both arms of the Mach–Zehnder interferometer are efficiently used, since they change the phase of the optical signal in opposite directions, which reduces by half the length of the modulator.

In the microwave calculation, it was taken into account that the thickness of the depletion region depends on the concentration of the dopant and the value of the reverse bias voltage. In particular, for $N_A = 3 \times 10^{17}$ cm^{-3} and $N_D = 14 \times 10^{17}$ cm^{-3}, when applying a reverse bias voltage of $V = 4$ V, the total thickness of the depletion region in the p–n junction will be ~0.18 μm, of which 0.15 μm corresponds to the region of holes, and 0.03 μm corresponds to the region of electrons.

Numerical simulation of the propagation of a quasi-TEM microwave in an electrode structure with p–n junctions shows that its properties depend on the magnitude of the reverse bias, which affects the size of the depletion region and, therefore, the capacitance of the p–n junction. In particular, with a reverse bias of 5 V, an impedance value close to 50 Ω can be obtained, which is important for matching with a 50-Ω external circuit. In addition, to describe the operation of an EO modulator, the attenuation of a microwave wave and its effective refractive index, which determine its operating frequency band, are of great importance [3]. The influence of these factors is described by the expression:

$$M_{RF}(F) = \exp(-\alpha_N L/2) \times \left[\frac{\sinh^2(\alpha_N L/2) + \sin^2(\xi L/2)}{(\alpha_N L/2)^2 + (\xi L/2)^2}\right]^{1/2}, \quad (2)$$

where L is the length of the active part of the modulator; $\xi = 2\pi F \times (N_{RF} - N_m)/c_0$; c_0 is the speed of light in vacuum; N_{RF} and N_m are the effective refractive indices for the microwave and for the fundamental mode of the optical wave; F is the microwave frequency; $\alpha_N = \alpha/(20 \log e)$; and α is the microwave attenuation (dB cm^{-1}). The general frequency characteristic of the EO modulator will be determined by the product of factors due to the p–n junction (1) and the microwave (2):

$$M(F) = M_{pn}(F) M_{RF}(F). \quad (3)$$

Using the microwave calculation data and expression (3), we found the main contributions that determine the microwave bandwidth for the travelling-wave EO modulator, as well as a number of other important parameters (Table 2). In this case, we considered the optical frequency band (ΔF), which corresponds to the criterion $M(\Delta F) = 0.5$. It is interesting to note that for long EO modulators that can operate at frequencies not exceeding 20 GHz, the main factor limiting the frequency band is the microwave attenuation. For shorter and, therefore, higher-frequency modulators, the main limiting factor is due to the velocity mismatch between the optical wave and microwave. Note that for our modulator design, transients in the p–n junction limit the frequency band insignificantly. If the characteristic frequency bands for the microwave contribution (ΔF_{RF}) and the contribution from the p–n junction (ΔF_{pn}) are known, the resulting band can be found from the empirical relation obtained from the numerical analysis of expressions (1)–(3):

$$(1/\Delta F)^{1.6} = (1/\Delta F_{RF})^{1.6} + (1/\Delta F_{pn})^{1.6}. \quad (4)$$

It is important to note that this type of the electro-optical modulator has good functional characteristics. In particular, at a voltage of 5 V, a modulator 0.17 cm long will have an optical frequency band ~50 GHz wide. By increasing the

Table 2. Microwave parameters of the electro-optical modulator at vertical p–n junctions with a reverse bias voltage of –5 V. The electrode width is 12 μm, providing an impedance of 50 Ω at this bias.

V_{max}/V	dV/V	L/cm	L_{RF}/dB	N_{RF}	ΔF_{RF}/GHz	ΔF_{NRF}/GHz	ΔF_{loss}/GHz	ΔF_{pn}/GHz	ΔF_{tot}/GHz	Z/Ω	L_{opt}/dB	$V_\pi L$ /V cm
1	1	0.501	10.7	5.499	11.6	14.8	20.1	243.0	11.5	39.7	4.07	1.001
2	2	0.305	22.8	4.942	22.3	33.0	33.8	285.3	22.1	43.4	2.37	1.222
3	3	0.232	35.1	4.617	32.4	56.8	44.4	303.5	31.8	46.0	1.73	1.392
4	4	0.192	47.5	4.365	42.4	105.7	54.6	297.1	41.2	48.4	1.38	1.538
5	5	0.172	57.2	4.186	50.8	160.0	62.2	420.4	49.7	50.3	1.20	1.719
6	6	0.159	65.3	4.048	58.3	223.3	68.8	400.0	56.7	51.9	1.09	1.904
7	7	0.148	74.2	3.912	66.2	339.9	75.4	358.3	63.5	53.6	0.99	2.065
5	3	0.393	18.73	4.2935	25.55	37.52	37.85	420.4	25.37	49.43	2.83	2.36
6	3	0.501	13.89	4.2016	22.24	30.888	34.06	400	22.11	50.69	3.51	3.008

Note: V_{max} and dV are the maximum value (at which the microwave properties are analysed) and the amplitude of the control voltage change; L is the length of the active part of the modulator operating in the push–pull regime; L_{loss} is the microwave loss; N_{RF} is the effective index of refraction of a microwave; ΔF_{RF} is the total contribution of the microwave to the width of the optical band of the EO modulator; ΔF_{NRF} is the contribution to the modulator bandwidth due to the velocity mismatch between the optical wave and microwave; ΔF_{loss} is the contribution to the modulator bandwidth due to microwave losses; ΔF_{pn} and ΔF_{tot} is the resulting modulator frequency band; Z is the wave impedance at maximum frequency; L_{opt} is the internal optical loss due to the presence of the p–n junction; and $V_\pi L$ is the product of half-wave voltage and the length of the modulator active part.

Table 3. Microwave parameters of the modified version of the electro-optical modulator based on vertical p–n junctions with a reverse bias voltage of –3 V. The electrode width is 12 μm, providing an impedance of 50 Ω at this bias.

V_{max}/V	dV/V	L/cm	L_{RF}/dB	N_{RF}	ΔF_{RF}/GHz	ΔF_{NRF}/GHz	ΔF_{loss}/GHz	ΔF_{pn}/GHz	ΔF_{tot}/GHz	Z/Ω	L_{opt}/dB	$V_\pi L$ /V cm
1	1	0.553	8.8	5.664	10.1	12.9	20.8	251.0	10.1	42.5	3.33	1.105
2	2	0.331	19.4	5.054	20.1	28.2	32.0	287.0	19.9	46.7	1.88	1.324
3	3	0.249	31.0	4.687	29.9	48.1	42.0	307.0	29.5	49.9	1.34	1.492
4	4	0.207	41.9	4.440	38.9	78.2	51.3	322.0	38.1	52.5	1.07	1.660
5	5	0.183	52.3	4.228	47.4	140.5	59.2	414.0	46.5	54.9	0.91	1.831
6	6	0.168	60.8	4.081	54.4	225.1	65.0	439.0	53.3	56.8	0.81	2.016
7	7	0.157	68.98	3.9489	61.28	363.96	70.52	438	59.69	58.68	0.74	2.193
4	3	0.332	21.77	4.4995	26.18	39.224	39.05	322	25.89	51.93	1.79	1.993

Note: The notations are the same as in Table 2.

length L of the active part of the modulator, it is possible to reduce the control voltage, but at the same time, the operating frequency band, as well as the wave impedance, are simultaneously reduced.

In principle, the application of a bias voltage (see the bottom two lines in Table 2) can provide a wave impedance close to 50 Ω, but at the same time, the modulation efficiency is significantly reduced (see the $V_\pi L$ value) and the frequency band width decreases. At the same time, if the manufacturing technology is slightly changed and the doping level of the upper part of the ridge is reduced to a level $N_D = 5 \times 10^{17}$ cm^{-3} (n_c in Fig. 3), the depletion region in the vicinity of the waveguide ridge will expand, which will reduce the total capacitance of the p–n junction and provide the condition for achieving a wave impedance of 50 Ω at a lower voltage (3 V). The calculation results for the modified version of the EO modulator are given in Table 3. It can be seen that such a 50-Ω three-volt modulator 0.25 cm long will already have an operating frequency band ~30 GHz wide, as well as significantly greater control efficiency ($V_\pi L$ = 1.5 V cm). Moreover, it is possible to create modulators with an operating voltage of 1 V and 2 V and, therefore, with moderate frequency bands (10 and 20 GHz, see Table 3).

Thus, when designing the EO modulator based on reverse p–n junctions in silicon, it is necessary to take into account the optical and microwave properties of its structure systematically. The construction parameters of the modulator radically depend on the operating frequency band intended for use and on the control voltage. Under these conditions, by optimising the structure parameters, it can be achieved that the modulator on vertical p–n junctions, even for a large-aperture optical beam (designed to transmit high-power radiation), will have technical parameters comparable to those of the best EO modulators of alternative designs [18–24]. In particular, such a modulator for the operating frequency band of 50 GHz with a control voltage of 5 V will have a total length of 7 mm and internal losses of ~4 dB, which are the sum of losses on the MMI elements 1 × 2 and 2 × 2 (~0.3 dB), losses in the active part of the modulator (~1.2 dB at a bias voltage of 5 V) and losses due to imperfections in the waveguide boundaries (~2.1 dB = 0.7 cm × 3 dB m^{-1}).

6. Conclusions

In the course of the numerical analysis, the suboptimal parameters were determined for the formation of the structure of the vertical p–n junction in a optical silicon ridge waveguide. They provide the making of a compact electro-optical travelling-wave modulator (total length 7 mm) with an operating voltage of ~5 V (for push–pull operation), an active electrode length of 1.7 mm and internal losses of less than 4 dB (for a bias voltage of 5 V). The modulator impedance is matched with a 50-Ω load at a frequency of 50 GHz and uses the optical scheme of the Mach–Zehnder interferometer with MMI elements 1 × 2 and 2 × 2, which provide an operating point without additional bias voltage. A modified modulator with a 50-Ω coplanar line impedance and a modified donor doping profile can operate in the 30 GHz frequency band with a control voltage of 3 V.

It is shown that, in solving the problem of optimising the parameters of a silicon EO modulator, it is necessary to proceed from the required frequency band and operating voltage, and in the process of appropriate numerical analysis to take into account the optical and microwave properties of its semiconductor and electrode structures in a systematic way. The obtained results can be used in the development of electro-optical modulators and optoelectronic elements for optical communication, radio photonics, as well as data processing and transmission systems.

Acknowledgements. The authors thank Synopsys, Inc. [33] for providing licensed software from RSoft for computer modelling of our structures. This work was supported by the Ministry of Science and Higher Education of the Russian Federation (Project Unique Identifier RFMEFI58117X0026).

References

1. Kaminow I. *IEEE Trans. Microw. Theory Tech.*, **23**, 57 (1975).
2. Chen A., Murphy E.J. *Broadband Optical Modulators: Science, Technology, and Applications* (Boca Raton: CRC Press, 2011).
3. Wooten E.L. et al. *IEEE J. Sel. Top. Quantum Electron.*, **6** (1), 69 (2000).
4. Liu J. et al. *RSC Advances*, **5**, 15784 (2015).
5. Zhang X. et al. *J. Lightwave Technol.*, **34**, 2941 (2016).
6. Lauermann M. et al. *J. Lightwave Technol.*, **33**, 1210 (2015).
7. Leuthold J. et al. *IEEE J. Sel. Top. Quantum Electron.*, **19**, 114 (2013).
8. Li B., Vemagiri J., Dinu R. *J. Lightwave Technol.*, **27**, 606 (2009).
9. Abedi K., Vahidi H. *Frontiers Optoelectron.*, **6**, 290 (2013).
10. Wang L.D. et al. *Appl. Phys. A*, **122**, 1 (2016).
11. Takahashi S. et al. *J. Lightwave Technol.*, **27**, 1045 (2009).
12. Denisyuk I.Yu., Burunkova Yu.E., Pozdnyakova S.A., Balya V.K., Zhuk D.I., Fokina M.I. *Opt. Spectrosc.*, **119** (4), 719 (2015) [*Opt. Spektrosk.*, **119** (4), 691 (2015)].
13. Mikerin S.L., Plekhanov A.I., Simanchuk A.E., Yakimanskii A.V., Martynenkov A.A., Valisheva N.A. *Optoelectron., Instrumen. Data Process.*, **54** (4), 385 (2018) [*Avtometriya*, **54** (4), 78 (2018)].
14. Tsarev A., Taziev R., Heller E., Chalony M. *Photon. Nanostruct. Fundament. Applicat.*, **25**, 31 (2017).

15. Juodawlkis P.W., O'Donnell F.J., Bailey R.J., Plant J.J., Ray K.G., Oakley D.C., Napoleone A., Watts M.R., Betts G.E. *Proc. SPIE*, **5435**, 0277 (2004).
16. Mitchell P., Longone R., Janssen A., Garrett B., Luo J.K.J. *Optoelectr. Advanc. Mater.*, **12**, 965 (2010).
17. Tsarev A.V., Taziev R.M. *Quantum Electron.*, **49**, 266 (2019) [*Kvantovaya Elektron.*, **49**, 266 (2019)].
18. Soref R. *IEEE J. Sel. Top. Quantum Electron.*, **12**, 1687 (2006).
19. Jalali B., Fathpour S. *J. Lightwave Technol.*, **24**, 4600 (2006).
20. Reed G.T. *Silicon Photonics – the State of the Art* (New York: John Wiley & Sons Ltd, 2008).
21. Wang J. *CMOS-Compatible Key Engineering Devices for High-Speed Silicon-Based Optical Interconnections* (New York: Springer, 2019).
22. Witzens J. *Proc. IEEE*, **106**, 2158 (2018).
23. Pinguet T. et al. *Proc. IEEE*, **106**, 2281 (2018).
24. Reed G.T., Mashanovich G., Gardes F.Y., Thomson D.J. *Nat. Photonics*, **4**, 518 (2010).
25. Green W.M.J., Rooks M.J., Sekaric L., Vlasov Y.A. *Opt. Express*, **15**, 17106 (2007).
26. Soref R., Bennett B. *IEEE J. Quantum Electron.*, **23**, 123 (1987).
27. Liu A., Liao L., Rubin D., Nguyen H., Ciftcioglu B., Chetrit Y., Izhaky N., Paniccia M. *Opt. Express*, **15**, 660 (2007).
28. Feng N.N., Liao S., Feng D.Z., Dong P., Zheng D., Liang H., Shafiiha R., Li G., Cunningham J.E., Krishnamoorthy A.V., Asghari M. *Opt. Express*, **18**, 7994 (2010).
29. Tu X.G., Liow T.Y., Song J.F., Yu M.B., Lo G.Q. *Opt. Express*, **19**, 18029 (2011).
30. Gardes F.Y., Thomson D.J., Emerson N.G., Reed G.T. *Opt. Express*, **19**, 11804 (2011).
31. Thomson D.J., Gardes F.Y., Liu S., Porte H., Zimmermann L., Fedeli J.M., Hu Y., Nedeljkovic M., Yang X., Petropoulos P., Mashanovich G.Z. *IEEE J. Sel. Top. Quantum Electron.*, **19**, 85 (2013).
32. Reed G.T., Mashanovich G.Z., Gardes F.Y., Nedeljkovic M., Hu Y., Thomson D.J., Hsu S.S. *Nanophotonics*, **3**, 229 (2014).
33. Liow T.-Y., Song J., Tu X., Lim A.E.-J., Fang Q., Duan N., Yu M., Lo G.-Q. *IEEE J. Sel. Top Quantum Electron.*, **19** (2013).
34. https://www.synopsys.com/optical-solutions/rsoft.html, single license (2018).
35. https://www.cst.com/products/cstmws, single license (2017).
36. https://www.ansys.com/products/electronics/ansys-hfss, single license (2018).
37. Tsang H.K., Liu Y. *Semicond. Sci. Technol.*, **23**, 064007 (2008).
38. Tsarev A.V., Taziev R.M. *Proc. 14th Intern. Sci.Techn. Conf. (APEIE)* (Novosibirsk, 2018) Vol. 1/2, p. 306.
39. Ghione G. *Semiconductor Devices for High-Speed Optoelectronics* (Cambridge: Cambridge Univ. Press, 2009).